A THREE VARIABLE AUTONOMOUS PHASE MODEL FOR NEURONAL PARABOLIC BURSTING.

STEVEN M. BAER
Department of Mathematics, Arizona State University
Tempe, Arizona 85287-1804, U.S.A.

JOHN RINZEL
Mathematical Researc Branch, N.I.H.
Bethesda, M.D. 20892, U.S.A.

HUMBERTO CARRILLO
Laboratorio de Dinamica No Lineal
Facultad de Ciencias UNAM
Mexico 04510 D.F.

In

DIFFERENTIAL EQUATIONS WITH APLICATIONS TO BIOLOGY AND INDUSTRY

IN MEMORY OF STRAVOS BUSENBERG

Editors: M. Martelli, E. Cooke, E. Cumberbactch, B. Tang and H. Thiem

Pages 1-11. World Scientific, Singapore, 1996

A THREE-VARIABLE AUTONOMOUS PHASE MODEL FOR NEURONAL PARABOLIC BURSTING

STEVEN M. BAER
Department of Mathematics, Arizona State University
Tempe, Arizona 85287-1804, U.S.A.

JOHN RINZEL
Mathematical Research Branch, NIH, Bethesda, MD 20892

HUMBERTO CARRILLO
Laboratorio de Dinamica No Lineal, Facultad de Ciencias, UNAM, Mexico 04510 D.F.

ABSTRACT

Bursting is characterized by alternations between phases of rapid spiking and slowly varying potential. A simple three-variable phase model is considered to study endogenous parabolic bursting, a class of burst activity observed experimentally in excitable neuronal membrane. Rapid spiking is represented canonically by a one-variable phase equation that is coupled bi-directionally to a two-variable slow system. The model is analyzed using quasi steady-state assumptions and formal averaging. A reduced system is derived to explore where the system exhibits bursting, steady-states, continuous and modulated spiking. It is found that the relative speed of activation and inactivation of the slow variables strongly influences the burst pattern as well as other dynamics, and there exists bistability of solutions between continuous spiking and bursting. Although the phase model is simple, it captures dynamical features of more complex biophysical models.

1. Introduction

Some cells known as bursting pacemakers fire with a pattern that alternates between an active phase of rapid oscillations and a silent phase of slowly changing membrane potential. Bursting oscillations have been observed in neuronal ensembles and in isolated neurons [11]. Bursting requires at least two different time scales, one on the scale of fast oscillations (1 to 10 milliseconds) and the other on the scale of slow modulations (10^{-1} to 10 seconds). An endogenous (or autonomous) burster is one in which the slow and fast systems are coupled bi-directionally; the fast drives the slow and the slow drives the fast. Mathematical models of endogenous bursting mechanisms are often modifications of the Hodgkin-Huxley model [12] with additional variables to account for the slowly modulated activity [18,21,14,19].

Figure 1 shows two different types of endogenous burst patterns: a square-wave burster (Fig. 1a) and a parabolic burster (Fig. 1b). The square-wave burster shows a relaxation-like character. The mean membrane potential jumps discontinuously when spiking begins and the spike frequency decreases at the end of the active phase. This pattern is characteristic of electrical bursting activity observed

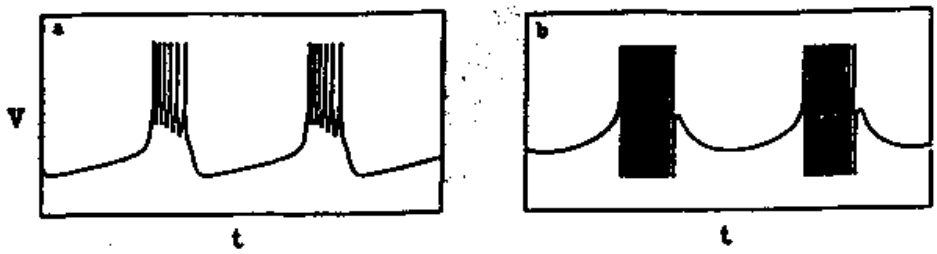

Figure 1. Two kinds of burst patterns. (a) A square-wave burster computed using the Morris and Lecar model (from Rinzel and Ermentrout [20]) (b) A parabolic burst pattern generated from the phase-burster model (1)-(3) with parameter values $\epsilon_x = 0.0050$, $\epsilon_y = 0.0015$, $a = 2$, $b = 5$, $I = -1.65$, $p_x = -0.3$, $p_y = -0.3$, and $V = \sin\theta(t)$.

in insulin-secreting β-cells of the islet of Langerhans in the pancreas [1]. There have been numerous Hodgkin-Huxley-type models exploring the biophysical mechanisms underlying bursting in β-cells and recently singular perturbation methods have been applied to this class of models [23,17,22]. The parabolic burster (Fig. 1b) rides on a smooth sinusoidal-like slow wave. The burst is called parabolic because the instantaneous spike frequency is low at both the beginning and end of an active phase. The R-15 neuron in the abdominal ganglion of *Aplysia* is an example of a parabolic burster and has been modeled by Plant [18] and studied qualitatively and numerically by others [21,4,5]. Parabolic bursting depends on there being at least two slow variables (for opposing effects: to promote or suppress rapid spike generation). In contrast, square-wave bursters need only one slow variable but with the requirement that the fast variable subsystem exhibit bistability [20]. Recently, Baer, Rinzel and Carrillo [2] developed a simplified three-variable phase model for endogenous parabolic bursting, namely

$$\dot{\theta} = 1 - \cos\theta + A(x,y) \tag{1}$$

$$\dot{x} = \epsilon_x [x_\infty(\theta) - x] \tag{2}$$

$$\dot{y} = \epsilon_y [y_\infty(\theta) - y] \tag{3}$$

where ϵ_x, ϵ_y are parameters representing speed of activation and inactivation (usually of order less that one), and x_∞, y_∞ are 2π-periodic functions of θ that strictly increase for $-\pi/2 \le \theta \le 0$. Here,

$$x_\infty(\theta) = \sin(p_x + \theta) \tag{4}$$

$$y_\infty(\theta) = \sin(p_y + \theta) \tag{5}$$

where p_x and p_y are constants. Sinusoids are chosen to keep the model simple and analytic, but other forms are possible. The slow subsystem, driven by θ, feeds back to the fast subsystem to provide bi-directional coupling through the activation function $A(x,y)$ defined by

$$A(x,y) = \tanh(ax - by + I), \tag{6}$$

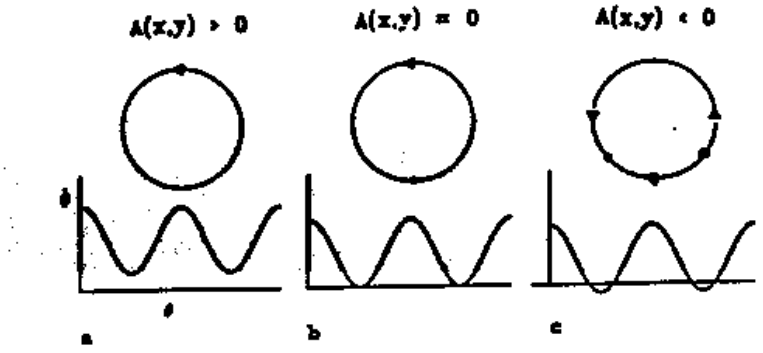

Figure 2. The fast subsystem is governed by ring dynamics. The curves plot the right hand side of Eq. (1) over two periods (4π). The rings represent the dynamics of θ for the three cases A positive, zero, and negative. Recall that A is coupled bi-directionally to θ through x and y. (a) When $A(x,y) > 0$, $d\theta/dt$ is always positive. The phase θ increases through multiples of 2π on the ring, corresponding to fast oscillations. (b) The case $A(x,y) = 0$ is analogous to a homoclinic bifurcation boundary in Plant's model. (c) When $A(x,y) < 0$, the phase θ has two singular points every 2π, one stable and the other unstable; θ slowly tracks the stable one (moduli 2π) as x and y slowly change.

where $a > 0$, $b > 0$. The net externally applied stimulus I is the primary control variable. Bursting occurs when the slow system Eqs. (2)-(3) sweeps $A(x,y)$ back and forth across $A = 0$. When $-1 < A < 0$ (silent region), θ is attracted to a slowly varying steady-state θ_s. When $0 < A < 1$ (active region), Eq. (1) destabilizes and θ respectively increases with time scale $O(1)$ through multiples of 2π, corresponding to repetitive spiking. As A decreases toward 0, the cycle time for θ becomes infinite. The burst pattern shown in Fig. 1b is computed with Eqs. (1)-(6), using $\sin\theta$ to represent the membrane potential.

The fast system is characterized using ring dynamics (see Fig. 2) [8]. Bursting oscillations occur when the slow variables x and y cause the activation function $A(x,y)$ to sweep back and forth across $A = 0$. When $A > 0$ the phase angle θ on the ring (see Fig. 2a) increases through multiples of 2π, corresponding to repetitive spiking. When $A = 0$, saddle nodes exist at multiples of 2π in Eq. (1) (see Fig. 2b), and for $A < 0$ there are two singular points for each multiple of 2π; a stable node and a saddle node (Fig. 2c). When $A < 0$, θ tracks a slowly varying stable manifold given by $\theta_s(x,y)$. As for this ring model, the detailed models have an invariant circle in phase space; as previously recognized for parabolic bursters, [21,8] burst trajectories pass through a SNIC (saddle node on an invariant circle) bifurcation both at the beginning and end of the active phase.

This paper is a selective survey of a longer paper by Baer, Rinzel and Carrillo [2], with the difference here being a stronger emphasis on the model's global bifurcation structure. In Section 2 the method of averaging is used to reduce the full model to an analytically accessible set of differential equations on the time scale of the slow oscillations. In Section 3 bifurcation diagrams for the reduced system are computed.

From the bifurcation structure of the reduced system conditions are identified for bistable solutions, modulated spiking, and more complex dynamics where formal averaging breaks down. Section 4 is discussion.

2. The Reduced System

In this section the dynamics of Eqs. (1)-(3) are approximated by a reduced system of differential equations that exploit disparities between the fast and slow subsystems.

If $A < 0$, solutions to Eqs. (1)-(3) rapidly approach the manifold

$$\theta_s(x,y) = -\arccos(1 + A(x,y)), \tag{7}$$

at least to leading order in ϵ_x and ϵ_y [13]. The function $\theta_s(x,y)$ constitutes a stable two dimensional slow manifold of the system [24]. The slow trajectory (x,y) in the silent region is then given by the quasistatic approximation

$$\frac{dx}{dt} = \epsilon_x \left[x_\infty(\theta_s(x,y)) - x\right] \tag{8}$$

$$\frac{dy}{dt} = \epsilon_y \left[y_\infty(\theta_s(x,y)) - y\right]. \tag{9}$$

For $A > 0$, the slow dynamics in the oscillatory region, derived from formal averaging, is governed by

$$\frac{dx_{av}}{dt} = \epsilon_x \left[\overline{x}_\infty(A(x_{av}, y_{av})) - x_{av}\right] \tag{10}$$

$$\frac{dy_{av}}{dt} = \epsilon_y \left[\overline{y}_\infty(A(x_{av}, y_{av})) - y_{av}\right]. \tag{11}$$

where,

$$\overline{x}_\infty(A) = \frac{1}{T(A)} \int_0^{2\pi} \frac{x_\infty(\theta)}{1 - \cos\theta + A} d\theta \tag{12}$$

$$= \left[(A+1) - \sqrt{(A+1)^2 - 1}\right] \sin p_x \tag{13}$$

$$\overline{y}_\infty(A) = \frac{1}{T(A)} \int_0^{2\pi} \frac{y_\infty(\theta)}{1 - \cos\theta + A} d\theta. \tag{14}$$

$$= \left[(A+1) - \sqrt{(A+1)^2 - 1}\right] \sin p_y. \tag{15}$$

Here T is the slowly varying period, found by integrating (1) from $\theta = 0$ to 2π, while holding A fixed:

$$T(A) = \int_0^{2\pi} \frac{d\theta}{1 - \cos\theta + A}$$

$$= \frac{2\pi}{\sqrt{(A+1)^2 - 1}}. \tag{16}$$

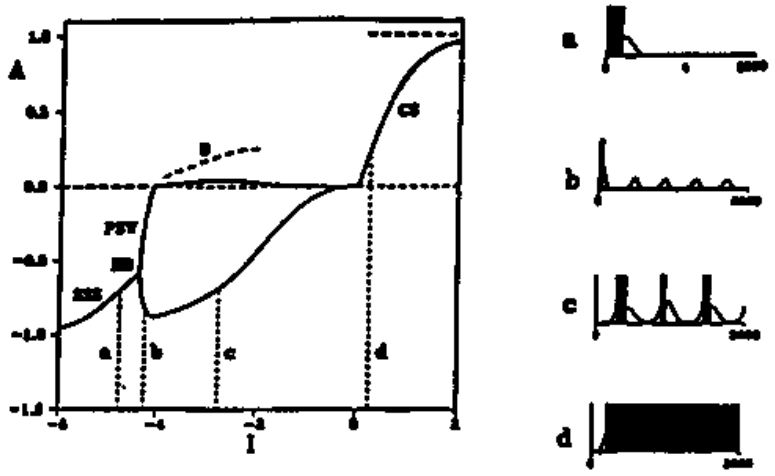

Figure 3. Bifurcation structure of the phase burster for $\epsilon_y \ll \epsilon_x$, computed from the reduced system: Eqs. (8)-(9) and (10)-(11); $\epsilon_x = 0.001$, $\epsilon_y = 0.0012$, $a = 2$, $b = 5$, $p_x = 1.3$, $p_y = 0.4$. The time courses for values of I labeled (a-d) are displayed in the panels.

Together, the quasi-static (8)-(9) and averaged equations (10)-(11), constitute the reduced system for the phase burster (1)-(3). Its solutions are continuous and differentiable for $A \neq 0$. As $A \to 0$ the component systems match asymptotically (compare Eqs. (13)-(15) for $A = 0$ with Eqs. (4)-(5) for $\theta = 0$).

The reduced system can be analyzed in the phase plane since its constituent subsystems are each second-order [2]. It has dynamics similar to other two variable models of excitability, such as the FitzHugh-Nagumo [10] and Morris-Lecar [16] equations; e.g., super and subcritical Hopf bifurcations, saddle nodes, and intervals of repetitive activity. Furthermore, when $\epsilon_y \ll \epsilon_x$ or vice versa, the reduced system has singular behavior and relaxation oscillator properties [15,9]. In the next section the dynamics of the phase burster is analyzed from the bifurcation structure of the reduced system.

3. Bifurcation Structure of the Reduced System

The reduced system is now employed to determine parameter values (corresponding to the full model) that bracket lower and upper thresholds for bursting, steady states, continuous and modulated spiking. Also, conditions for bistability of solutions between continuous spiking and bursting are found.

The bifurcation structure of the reduced system, for $\epsilon_y \ll \epsilon_x$, is shown in Fig. 3. The net stimulus I is chosen as the primary control parameter. The values of I indicated by (a-d) correspond to the trajectories in Fig. 3(a-d). At the lower range of the net stimulus ($I = -6$), the activation function is in the silent region ($A < 0$). Solution trajectories converge to a stable steady state (SSS) as shown in (a). There

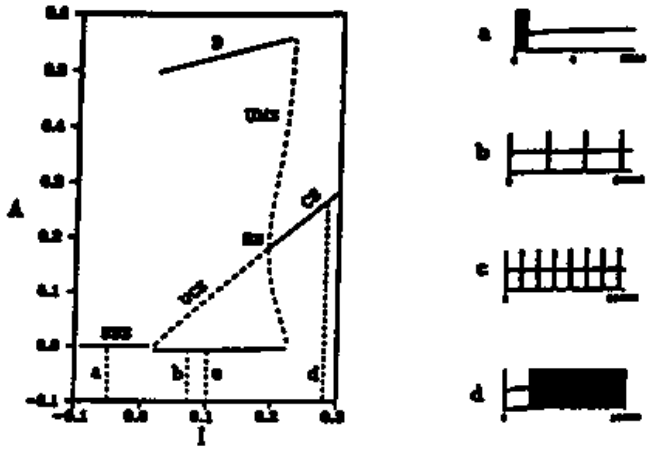

Figure 4. Bifurcation structure of the phase burster for $\epsilon_x \ll \epsilon_y$, computed from the reduced system. Parameter values the same as in Fig. 3, except $\epsilon_x = 0.002$ and $\epsilon_y = 0.008$. The time courses for values of I denoted by (a-d) are displayed in the panels.

is a (supercritical) Hopf bifurcation to periodic solutions at HB ($I \doteq -4.42$). Here, the activation function is negative, so the full system exhibits pure slow waves PSW at (b). The periodic branch is near vertical due to the disparate time scales of the slow system. Consequently, for I just to the right of HB the slow waves have small amplitude relaxation oscillator properties, such as the sawtooth wave pattern analyzed by Baer and Erneux [3]. For larger values of I at (c), the activation function continues to oscillate but sweeps positive for a fraction of its period, which corresponds to bursting in the full model. The dashed curve B is the fraction of time that the burst solution spends in the active phase (use same scale as A); time spent in the active phase increases as I increases.

Over the interval $-2 < I < 0$ the activation function spends much of its time in the vicinity of $A = 0$, and the leading order estimate given by averaging breaks down (In cases where the slow trajectory remains near a SNIC curve, like $A = 0$, one could apply the analytic method developed by Ermentrout [7] to approximate the slow trajectory.) Numerical solutions of the full system in this domain have complicated dynamics; as I approaches zero (the cusp) bursting and spiking become irregular. Hodgkin-Huxley like bursting models exhibit a similar transitional behavior. Finally, for I positive, the system spikes continuously CS. The horizontal dashed line above the CS curve indicates that the system eventually spends all its time in the active phase (see (d)).

When $\epsilon_x \ll \epsilon_y$ the bifurcation structure is quite different. Instead of a Hopf bifurcation from SSS to PSW, Fig. 4 shows that the system apparently goes directly from SSS to B through a homoclinic bifurcation. The dashed curve labeled UCS is an unstable steady-state branch, which corresponds to a branch of unstable contin-

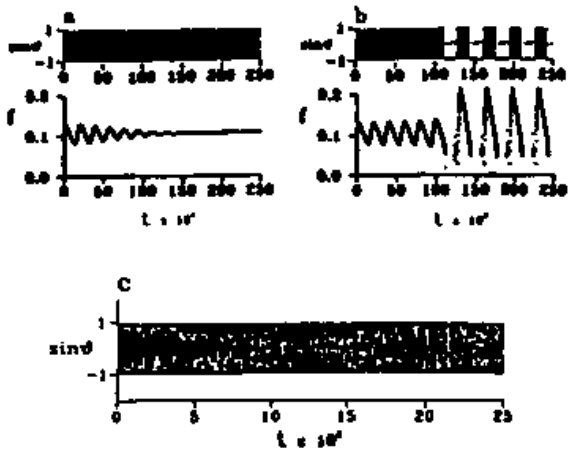

Figure 5. Bistable solutions for $\epsilon_z \ll \epsilon_y$. Same parameters as in Fig. 4 ($I = 0.24$), but all solutions are computed directly from the full model (1)-(3). (a) Top: in response to a small amplitude perturbation from stable continuous spiking the full system returns to continuous spiking through frequency modulated spiking, although on this time scale frequency modulations cannot be resolved (see (c) below). The frequency of fast oscillations f, plotted below as a function of time, decays to steady-state. (b) In response to a larger perturbation, modulated spiking grows (lower) until the onset of bursting. (c) Unstable modulated spiking: expanded view of the top time course in (a) for t between 0 and 2500. On this scale frequency modulation can be observed.

uous spiking solutions for the full system. At large stimulus values (d) the reduced system has a stable steady-state, therefore the full system spikes continuously (panel (d)). Unlike Fig. 3, there is a Hopf bifurcation for $A > 0$ rather than for $A < 0$. Just to the right of HB two kinds of stable solutions coexist: a stable steady-state and a large amplitude periodic solution. The stable steady-state corresponds to continuous spiking and the stable periodic solution corresponds to bursting, since A alternates sign each cycle (see Fig. 5 a and b, respectively). The bifurcation is subcritical, so the local periodic branch is unstable, and periodic solutions on this branch correspond to unstable modulated spiking UMS in the full system (see Fig. 5c). In this bifurcation structure there are no values for I that give rise to stable slow waves. To obtain stable modulated spiking would require a supercritical Hopf bifurcation for $A > 0$. A local bifurcation analysis (not provided here) of the averaged subsystem (10)-(11) demonstrates that the bifurcation is always subcritical. It is interesting to note that coexistence of bursting and continuous spiking behavior has been found in a parabolic burster model by Canavier et al [4].

The burst solutions at (b), in Fig. 4, has a silent phase over twice as long as the burst solution at (c). The longer silent phase at (b) is due to the fact that I is closer to a homoclinic point of bifurcation. This also explains why during the silent phase the time course appears flat. This feature, common to all panels in Fig. 4, is not usually associated with parabolic burst activity; typically, trajectories

characteristically ride on sinusoidal-like slow waves. Finally, for negative values of I, the system settles into a steady state (a).

4. Discussion

The phase burster exhibits dynamics remarkably similar to more complex models of parabolic bursting. The dynamics should not be identical for two reasons: first, the simple phase representation greatly simplifies the fast subsystem and second, the slow equations can vary from model to model. The phase burster's slow equations also have a very simple form.

The phase model may be viewed as a canonical description of more complex models, in much the same way the FitzHugh-Nagumo equations serve in studying features of the Hodgkin-Huxley system. To demonstrate this, consider Rinzel and Lee's model for a parabolic burst mechanism based on calcium-inactivation of a calcium conductance, which they call the Ca-Ca model [21]. The equations for the fast dynamics of the Ca-Ca model have a Hodgkin-Huxley like form:

$$\begin{aligned} C_m\dot{V} &= -\bar{g}_{Na}\, m_\infty^3(V)\, h\, (V - V_{Na}) - \bar{g}_K\, n^4\, (V - V_K) - \bar{g}_L\, (V - V_L) \\ &\quad -\bar{g}_{Ca-Ca} X\, H(Ca)\, (V - V_{Ca}) - \bar{g}_{K,0}(V - V_K) \qquad (17) \\ \dot{h} &= \lambda\, (h_\infty - h)/\tau_h \qquad (18) \\ \dot{n} &= \lambda\, (n_\infty - n)/\tau_n \qquad (19) \end{aligned}$$

Here, V denotes membrane potential (mV); h is a V-dependent, HH-like inactivation variable for Na-channels, and n is the activation of HH K-Channels. $H(Ca)$ is a nonlinear inactivation function which responds instantaneously to Ca. The slow dynamics is governed by

$$\begin{aligned} \dot{X} &= [X_\infty(V) - X]/\tau_X \qquad (20) \\ \dot{Ca} &= \rho\, [Ca_\infty(V, X, Ca) - Ca] \qquad (21) \end{aligned}$$

where X is an activation variable which controls the inward calcium conductance represented as $\bar{g}_{Ca-Ca} X\ H(Ca)$, and Ca is the slowly changing concentration of cytoplasmic free calcium which acts to depress or inactivate the fast spike generating system (17)-(19). In comparison to the phase burster model (1)-(3), X is analogous to x and Ca is analogous to y; with the important difference that Ca_∞ is a function of the two slow variables in addition to a fast variable, whereas y_∞ is a function of the fast variable θ only. The parameters and nonlinear functions for (17)-(21) are listed in the Appendix of Baer et al [2]. A more detailed description of the Ca-Ca model can be found in Rinzel and Lee [21]. Canavier et al [5] have also formulated a biophysical Ca-Ca model.

In Fig. 6 a burst solution to (17)-(21) is projected into the plane $Ca - X$ of slow variables. Figure 6 can be compared directly to Rinzel and Lee's Fig. 8 (which is computed with the same parameter values as Fig. 6). In this figure the averaged X and Ca-nullclines are included. These nullclines were computed using a numerical

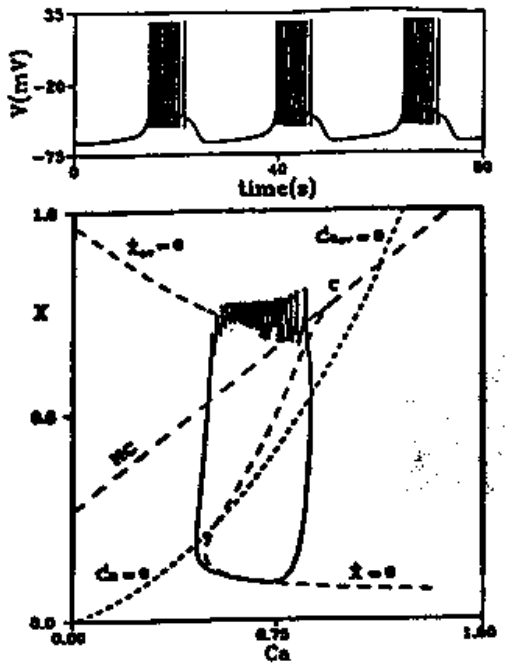

Figure 6. Burst solution of the Ca-Ca model follows the X_{ss}-nullcline in the active phase. Projection of solutions to Eqs. (17)-(21) onto plane $Ca - X$ of slow variables (from Baer et al [2]). The SNIC curve corresponds to a homoclinic orbit at a saddle-node point. (a) $\rho = 10^{-4}$ and $\tau_x = 235$ (same values as Fig. 8 in Rinzel and Lee [21]). The nullclines from the active and silent regions meet to form a cusp at C. (b) The trajectory follows even closer to the X_{ss}-nullcline when Ca and X are slowed down: $\rho = 10^{-5}$ and $\tau_x = 5000$.

procedure described by Smolen et al [22], which uses the bifurcation code AUTO [6] to find nullclines for the slow variables when the fast variables are periodic, by averaging over the fast oscillations. This procedure is time consuming and of course not necessary for the phase burster, since averaged equations can be derived in closed form. A prominent feature in Fig. 6 is the cusp formed where the X-nullcline from the silent region and its averaged counterpart meet along the SNIC curve. The Ca-nullcline also has a cusp on the SNIC boundary, but it is small and difficult to see in Fig. 6. Baer et al [2] have found that the phase burster model has a similar cusp-like structure in the phase plane.

Finally, the bifurcation structure of the Ca-Ca model is qualitatively similar to the supercritical structure in Fig. 3; i.e., stable steady states give rise to slow oscillations followed by bursting and continuous spiking as $1/K_c$ increases. The parameter K_c controls the Ca-nullcline, and as Rinzel and Lee point out, increasing K_c rotates the nullcline clockwise. Therefore, increasing $1/K_c$ drives the equilibrium point up through the cusp and over onto the oscillatory side, where the equilibrium

point becomes stable; this is the continuous spiking case. The reciprocal of K_c is proportional to the removal rate of calcium; a low removal rate corresponds to a stable steady state, a high rate continuous spiking. In this sense $1/K_c$ is analogous to our net stimulus parameter I. In Fig. 6, $\rho < 1/\tau_x$, which is consistent with inactivation (ϵ_y) being slower than activation (ϵ_x) in the phase model.

5. Acknowledgements

This research was partially supported by NSF-JOINT RESEARCH grant 8803573, grant from CONCYT and DGAPA (UNAM) Mexico for H. Carrillo, and for S.M. Baer DMS-9107538.

6. References

1. F. Ashcroft and P. Rorsman, *Prog. Biophys. Molec. Biol.* **54** (1989) 87.
2. S. M. Baer, J. Rinzel, and H. Carrillo, *J. Math. Biol.* **33** (1995) 309.
3. S. M. Baer and T. Erneux, *SIAM J. Appl. Math.* **52** (1992) 1651.
4. C. C. Canavier, D. A. Baxter, J. W. Clark, and J. H. Byrne, *J. Neurophysiol.* **69** (1993) 2252.
5. C. C. Canavier, J. W. Clark, and J. H. Byrne, *J. Neurophysiol.* **66** (1991) 2107.
6. E. Doedel, *Cong. Num.* **30** (1981) 265.
7. G. B. Ermentrout, *Neural Computation*, in press.
8. G. B. Ermentrout and N. Kopell, *SIAM J. Appl. Math.* **46** (1986) 233.
9. J. Grasman, *Asymptotic Methods for Relaxation Oscillations and Applications* (Applied Mathematical Sciences **63**) (Springer-Verlag, Berlin, 1987).
10. R. FitzHugh, in *Biological Engineering*, H. P. Schwan,ed. (McGraw Hill, New York, 1969).
11. B. Hille, *Ionic Channels of Excitable Membranes (2nd ed.)* (Sinauer Associates, Sunderland, MA, 1992), p. 126.
12. A. Hodgkin and A. Huxley, *J. Physiol. (Lond.)* **117** (1952) 500.
13. F. Hoppensteadt, *Trans. Amer. Math. Soc.* **123** (1966) 521.
14. J. Keizer, *Math. Biosc.* **90** (1988) 127.
15. J. Kevorkian and J. D. Cole, *Perturbation Methods in Applied Mathematics* (Applied Mathematical Sciences **34**) (Springer-Verlag, Berlin, 1981).
16. C. Morris and H. Lecar, *Biophys. J.* **35** (1981) 193.
17. M. Pernarowski, R. M. Miura, and J. Kevorkian, *SIAM J. Appl. Math.* **52** (1992) 1627.
18. R.E. Plant, *J. Math. Biol.* **11** (1981) 15.
19. J. Rinzel, in *Mathematical Topics in Population Biology, Morphogenesis, and Neurosciences* (Lect. Notes Biomath. **71**), E. Teramoto and M. Yamaguti, eds. (Springer-Verlag, New York, 1987).

20. J. Rinzel and G. B. Ermentrout, in *Methods in Neuronal Modeling: From Synapses to Networks*, C. Koch and I. Segev, eds. (MIT Press, Cambridge London, 1989).
21. J. Rinzel and Y. S. Lee, *J. Math. Biol.* **25** (1987) 653.
22. P. Smolen, D. Terman, and J. Rinzel, *SIAM J. Appl. Math.* **53** (1993) 861.
23. D. Terman, *SIAM J. Appl. Math.* **51** (1991) 1418.
24. A. N. Tikhonov, *Mat. Sb. Ns. (31)* **73** (1952) 575.